

Interplay between Hund's coupling and spin-orbit interaction on elementary excitations in Sr_2IrO_4

Jun-ichi Igarashi¹ and Tatsuya Nagao²

¹*Faculty of Science, Ibaraki University, Mito, Ibaraki 310-8512, Japan*

²*Faculty of Engineering, Gunma University, Kiryu, Gunma 376-8515, Japan*

(Dated: September 17, 2018)

We study the elementary excitations in 5d transition metal oxide Sr_2IrO_4 by calculating the particle-hole Green's function within the random phase approximation on an antiferromagnetic ground state in the two-dimensional multi-orbital Hubbard model. The obtained magnetic excitations of bound states show a characteristic dispersion in consistent with the experiments. In addition, two new types of excitations are found due to the interplay between spin-orbit interaction and Hund's coupling: a magnetic excitation as a bound state, which has energy gap at the Γ point, and an exciton as a resonant mode in the continuum of electron-hole pair creation.

Electron correlation effects on transition metals and their compounds have attracted much interest since the discovery of high- T_C cuprate superconductors. In the 3d transition metal ions, the spin orbit interaction (SOI) plays a minor role on the electronic structures, since it is usually much smaller than the on-site Coulomb interaction and the crystal field splitting. In the 5d transition metal ions, however, the SOI is one order of magnitude larger than that of the 3d systems while the Coulomb interaction becomes weaker due to the extended nature of the 5d electrons. Accordingly, the interplay between the electron correlation and the SOI is expected to bring about new intriguing phenomena. For this reason, much attention has recently been paid to Ir oxides such as Sr_2IrO_4 ¹⁻⁸ and Na_2IrO_3 .⁹⁻¹²

In particular, we focus on Sr_2IrO_4 , which consists of two-dimensional IrO_2 layers showing structural similarity to the parent compound of high- T_C cuprate La_2CuO_4 , and exhibits a canted antiferromagnetic (AFM) order below 230 K.¹⁻³ The energy of the e_g orbitals is estimated about 2 eV higher than that of the t_{2g} orbitals due to the large crystal field. Five 5d electrons are occupied per Ir atom, and one hole is sitting in the t_{2g} orbitals. Since the hole states have an effective orbital angular momentum ℓ equal to -1 , the lowest-energy states on the localized electron picture are doubly degenerate with the effective total angular momentum $j_{\text{eff}} = \frac{1}{2}$ under the SOI:^{13,14} $|\phi_{\pm}\rangle = \frac{1}{\sqrt{3}}(|yz, \mp\sigma\rangle \pm i|zx, \mp\sigma\rangle \pm |xy, \pm\sigma\rangle)$, where yz , zx , and xy designate t_{2g} orbitals, and spin component $\sigma = \uparrow$. By introducing the isospin operators acting on these states, the system is mapped onto the Heisenberg model, from which an insulating AFM phase is derived, consistent with the experiments.¹⁻³ Furthermore, it has been pointed out that the small anisotropic terms emerge in addition to the isotropic term, when Hund's coupling is taken into account in the second-order process in the strong coupling expansion.^{15,16}

Recently, resonant inelastic x-ray scattering (RIXS) experiment at the Ir L edge has detected the excitation spectra,¹⁷ whose low energy part follows the dispersion relation similar to the spin wave in the Heisenberg model on a square lattice. A notable point is that the exci-

tation energy at the M point is nearly half of that at the X point, in contrast to the situation in the undoped cuprates such as La_2CuO_4 ¹⁸ and $\text{Sr}_2\text{CuO}_2\text{Cl}_2$.¹⁹ It is known that the Heisenberg model with only the nearest neighbor exchange interaction gives the spin-wave energy at the M point nearly the same as that at the X point. The large energy difference in Sr_2IrO_4 requires the large farther neighbor exchange interactions in the Heisenberg model, which suggests the importance of itinerant character. The excitonic excitations are observed around 0.4-0.9 eV, not far above the magnetic excitations.¹⁷ This contrasts with the excitation spectra of undoped cuprates, where only the d-d excitations appear with the energies far above the spin wave excitations.^{18,19} In addition to these experimental facts, a study using the dynamical mean field theory has argued that the system is not the Mott insulator but the Slater insulator.²⁰ In contrast, a recent angle-resolved photoemission measurement suggests that the data are consistent with a Mott scenario rather than a Slater scenario.²¹

Under such circumstances, it may make sense to study elementary excitations from the intermediate coupling scheme based on the itinerant electron picture. In this paper, introducing the multi-orbital Hubbard model to describe the system, we calculate the particle-hole Green's function within the Hartree-Fock approximation (HFA) and the random phase approximation (RPA). We first confirm the obtained magnetic excitations as bound states show good agreement with the RIXS experiment.¹⁷ Furthermore, we find two kinds of new excitation modes emerge, which are attributed to the interplay between the SOI and Hund's coupling. One is the gap mode associated with the splitting of the magnetic excitation. Another is the exciton in the continuum of electron-hole pair excitation, whose dispersive behavior as a function of the momentum transfer shows in qualitative agreement with the RIXS experiment.

We employ the multi-orbital Hubbard model defined by the base states in the local coordinate frames rotated in accordance with the rotation of the oxygen octahedra surrounding an Ir atom with respect to the crystallo-

graphic c axis about 11° .^{22,23} It may be expressed as

$$H = H_{\text{kin}} + H_{\text{SO}} + H_{\text{I}}, \quad (1)$$

with

$$H_{\text{kin}} = \sum_{\langle i, i' \rangle} \sum_{n, n', \sigma} \left(t_{in, i'n'} d_{in\sigma}^\dagger d_{i'n'\sigma} + \text{H.c.} \right), \quad (2)$$

$$H_{\text{SO}} = \zeta_{\text{SO}} \sum_i \sum_{n, n', \sigma, \sigma'} d_{in\sigma}^\dagger (\mathbf{L})_{nn'} \cdot (\mathbf{S})_{\sigma\sigma'} d_{in'\sigma'}, \quad (3)$$

$$\begin{aligned} H_{\text{I}} &= U \sum_{i, n} n_{in\uparrow} n_{in\downarrow} \\ &+ J \sum_{i, n \neq n'} (d_{in\uparrow}^\dagger d_{in'\downarrow}^\dagger d_{in\downarrow} d_{in'\uparrow} + d_{in\uparrow}^\dagger d_{in'\downarrow}^\dagger d_{in\downarrow} d_{in'\uparrow}) \\ &+ \sum_{i, n < n'} [U' n_{in\sigma} n_{in'-\sigma} + (U' - J) n_{in\sigma} n_{in'\sigma}], \quad (4) \end{aligned}$$

where $d_{in\sigma}$ denotes the annihilation operator of an electron with orbital n ($= yz, zx, xy$) and spin σ at the Ir site i . The H_{kin} represents the kinetic energy with transfer integral $t_{in, i'n'}$. An electron on the xy orbital could transfer to the xy orbital in the nearest neighbor sites through the intervening O $2p$ orbitals, while an electron on the $yz(zx)$ orbital could transfer to the $yz(zx)$ orbital in the nearest-neighbor sites only along the $y(x)$ direction. The non-zero values of $t_{in, i'n'}$'s are assumed to be the same and denoted as t_1 . The crystal distortion makes the energy of the xy orbital different from that of the yz and zx orbitals, as well as the further neighbor transfer integrals with the xy orbital substantial, which effects are neglected. The H_{SO} represents the SOI of $5d$ electrons; $(\mathbf{L})_{nn'}$ represents the matrix element of the orbital momentum operator between the orbitals specified by n, n' , and $(\mathbf{S})_{\sigma\sigma'}$ represents the matrix element of spin angular momentum operators between the spin states specified by σ, σ' . The H_{I} represents the Coulomb interaction between electrons, which satisfies $U = U' + 2J$.²⁴ We use the values $U = 1.26$ eV, $\zeta_{\text{SO}} = 0.324$ eV, $t_1 = 0.324$ eV, and $J/U = 0 - 0.15$ in the following calculation.

We consider a unit cell j containing two atoms at $\mathbf{r}_i(j) = \mathbf{r}_j + \boldsymbol{\delta}_i$, where $\boldsymbol{\delta}_i = (0, 0)$ and $(a, 0)$ for sublattices A and B, respectively. Here a is a nearest neighbor distance. The Fourier transform of annihilation operator is defined in the half of the Brillouin zone called as the magnetic Brillouin zone (MBZ):

$$d_{\lambda n\sigma}(\mathbf{k}) = \sqrt{\frac{2}{N}} \sum_j d_{in\sigma} e^{-i\mathbf{k} \cdot \mathbf{r}_j}, \quad (5)$$

where j runs over $N/2$ unit cells and \mathbf{k} is the wave number. The sublattice A or B is discriminated by $\lambda = 1$ or 2 , respectively. With this definition together with abbreviations $\xi = (\lambda, n, \sigma)$ and $\xi' = (\lambda', n', \sigma')$, H_{kin} is rewritten as

$$H_{\text{kin}} = \sum_{\mathbf{k}\xi\xi'} d_{\xi}^\dagger(\mathbf{k}) \left[\hat{H}_{\text{kin}}(\mathbf{k}) \right]_{\xi, \xi'} d_{\xi'}(\mathbf{k}). \quad (6)$$

Then, we introduce the single-particle Green's function in a matrix form with 12×12 dimensions,

$$\left[\hat{G}(\mathbf{k}, \omega) \right]_{\xi, \xi'} = -i \int \langle T(d_\xi(\mathbf{k}, t) d_{\xi'}^\dagger(\mathbf{k}, 0)) \rangle e^{i\omega t} dt, \quad (7)$$

where T is the time ordering operator, and $\langle X \rangle$ denotes the ground-state average of operator X .

We follow the conventional procedure of the HFA with the help of the Green's function. The summation over \mathbf{k} is carried out by dividing the MBZ into 100×100 meshes to evaluate average values of density operators.²⁵ Assuming the staggered moment along the x -axis, we obtain a self-consistent solution of the AFM order consistent with the magnetic measurements.^{1,2} Both the orbital and spin moments are induced due to the strong SOI. For $J/U = 0.15$, we have $\langle S_x \rangle = \pm 0.112$ and $\langle L_x \rangle = \pm 0.435$. These values are compared with the average on the Kramers' doublet $|\frac{1}{2}, \pm \frac{1}{2}\rangle \equiv \frac{1}{\sqrt{2}}(|\phi_\pm\rangle \pm |\phi_\mp\rangle)$ defined with the quantization axis along the x axis, that is: $\langle \frac{1}{2}, \pm \frac{1}{2} | S_x | \frac{1}{2}, \pm \frac{1}{2} \rangle = \mp \frac{1}{6}$ and $\langle \frac{1}{2}, \pm \frac{1}{2} | L_x | \frac{1}{2}, \pm \frac{1}{2} \rangle = \mp \frac{2}{3}$. Note that the obtained AFM order in the local coordinate frames implies that the canted AFM order is realized in the global coordinate frame with concomitant weak ferromagnetic component.

The single-particle Green's function is expressed as

$$\hat{G}(\mathbf{k}, \omega) = \hat{U}(\mathbf{k}) \hat{D}(\mathbf{k}, \omega) \hat{U}(\mathbf{k})^{-1}, \quad (8)$$

with

$$[\hat{D}(\mathbf{k}, \omega)]_{j, j'} = \delta_{j, j'} \{ \omega - E_j(\mathbf{k}) + i\eta \text{sgn}[E_j(\mathbf{k})] \}^{-1}, \quad (9)$$

where $\text{sgn}[A]$ stands for a sign of quantity A and η denotes a positive convergent factor. The $E_j(\mathbf{k})$'s represent the energy eigenvalues within the HFA measured from the chemical potential. Figure 1 shows the single-particle energy as a function of \mathbf{k} along the symmetry lines. Each level is doubly degenerate in the MBZ. The conduction band mainly consists of the $j_{\text{eff}} = \frac{1}{2}$ character, and the energy gap is created by the AFM order, consistent with the previous studies.^{13,14,22}

Now we consider the particle-hole Green's function defined by

$$\left[\hat{Y}^{\text{T}}(q) \right]_{\xi_1 \xi'_1; \xi \xi'} = -i \int \langle T[(\rho_{\mathbf{q}\xi_1 \xi'_1}(t))^\dagger \rho_{\mathbf{q}\xi \xi'}(0)] \rangle e^{iq_0 t} dt, \quad (10)$$

with

$$\rho_{\mathbf{q}\xi \xi'} = \sqrt{\frac{2}{N}} \sum_{\mathbf{k}} d_{\xi}^\dagger(\mathbf{k} + \mathbf{q}) d_{\xi'}(\mathbf{k}), \quad (11)$$

where an abbreviation $q = (\mathbf{q}, q_0)$ is introduced for the energy q_0 and wave number \mathbf{q} . When $\mathbf{k} + \mathbf{q}$ lies outside the MBZ, it is implicitly reduced back to the MBZ by a reciprocal lattice vector. The $\hat{Y}(q)$ is a matrix with 144×144 dimensions. Collecting up the ladder diagrams within the RPA, we obtain

$$\hat{Y}^{\text{T}}(q) = \hat{F}(q) [\hat{I} + \hat{\Gamma} \hat{F}(q)]^{-1} = \left[\hat{F}(q)^{-1} + \hat{\Gamma} \right]^{-1}, \quad (12)$$

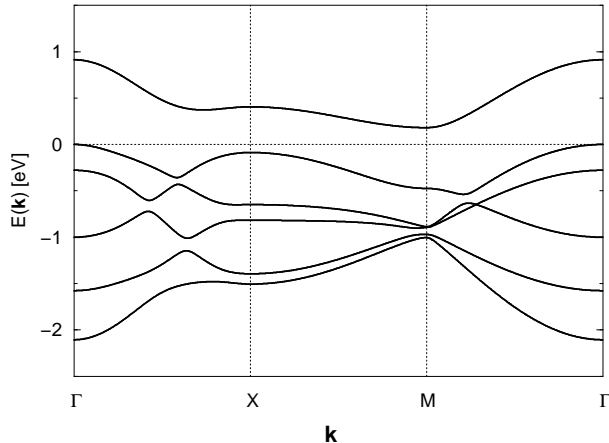


Figure 1: Single-particle energy along symmetry lines. Here, the special points Γ , X , and M refer to $\mathbf{k} = (0, 0)$, $(\pi, 0)$, and $(\frac{\pi}{2}, \frac{\pi}{2})$, respectively. $J/U = 0.15$. The origin of energy is set at the top of valence band.

where $\hat{\Gamma}$ represents the antisymmetric vertex, function²⁶ $[\hat{\Gamma}]_{\xi_2\xi'_2;\xi_1\xi'_1} = \Gamma^{(0)}(\xi_2\xi'_1;\xi_1\xi'_2)$. Function $\hat{F}(q)$ is given by

$$\begin{aligned} & [\hat{F}(\mathbf{q}, q_0)]_{\xi_2\xi'_2;\xi_1\xi'_1} \\ & \equiv -i \frac{2}{N} \sum_{\mathbf{k}} \int \frac{dk_0}{2\pi} [\hat{G}(\mathbf{k} + \mathbf{q}, k_0 + q_0)]_{\xi_2,\xi_1} [\hat{G}(\mathbf{k}, k_0)]_{\xi'_1,\xi'_2} \\ & = \frac{2}{N} \sum_{\mathbf{k},j,\ell} U_{\xi_2j}(\mathbf{k} + \mathbf{q}) U_{\xi_1j}^*(\mathbf{k} + \mathbf{q}) U_{\xi'_1\ell}(\mathbf{k}) U_{\xi'_2\ell}^*(\mathbf{k}) \\ & \times \left[\frac{[1 - n_j(\mathbf{k} + \mathbf{q})]n_\ell(\mathbf{k})}{q_0 - E_j(\mathbf{k} + \mathbf{q}) + E_\ell(\mathbf{k}) + i\eta} \right. \\ & \quad \left. - \frac{n_j(\mathbf{k} + \mathbf{q})[1 - n_\ell(\mathbf{k})]}{q_0 - E_j(\mathbf{k} + \mathbf{q}) + E_\ell(\mathbf{k}) - i\eta} \right], \end{aligned} \quad (13)$$

where $n_\ell(\mathbf{k})$ denotes the occupation number of the eigenstate with energy $E_\ell(\mathbf{k})$ given by the HFA. Using a relation $1/(\omega - E \pm i\eta) = P\{1/(\omega - E)\} \mp i\pi\delta(\omega - E)$ in the last line of Eq. (13), we can express $\hat{F}(q)$ as $\hat{F}(q) = \hat{F}_1(q) + i\hat{F}_2(q)$ with $\hat{F}_1(q)$ and $\hat{F}_2(q)$ being Hermitian matrices.

First, we search for the magnetic excitations below the continuous electron-hole creation. In evaluating Eq. (13), we sum over \mathbf{k} by dividing the MBZ into 300×300 meshes. Since $\hat{F}_2(q) = 0$ there, they come out as bound states. First we discuss on the Γ -point. Since $\hat{F}_1(0, q_0)$ is found to have zero eigenvalues, $\hat{F}_1(0, q_0)^{-1}$ does not exist. Hence, we determine the bound state by the divergent condition for Eq.(12). We find that one eigenvalue of Eq. (12) goes to as large as 10^4 in units of $(\text{eV})^{-1}$ with $q_0 \rightarrow 0$. It is taken as the divergence within the numerical errors. This mode with zero excitation energy may be a Goldstone mode. In addition, we find another divergence occurs at $q_0 = 0.057$ eV, indicating that two modes exist. For general values of \mathbf{q} , the bound states are determined by adjusting q_0 to give zero eigenvalue in $\hat{F}_1(q)^{-1} + \hat{\Gamma}$. We find two modes exist in the entire MBZ. Note that, if

Hund's coupling J is zero, the lowest eigenvalue is doubly degenerate, implying the absence of the split of modes. The wavefunction of the magnetic excitation is given by the eigenfunction for the zero eigenvalue of $\hat{F}(q)^{-1} + \hat{\Gamma}$, which is composed of a direct product of the particle and hole states. The particle sectors are mainly $|\frac{1}{2}, +\frac{1}{2}\rangle$ and $|\frac{1}{2}, -\frac{1}{2}\rangle$ with $\lambda = 1$ and 2 , respectively, reflecting the character of the conduction band.

Figure 2 shows the excitation energy $\omega_B(\mathbf{q})$ for \mathbf{q} along high symmetry directions. The (black) circles and (red) squares represent the Goldstone and gap modes, respectively. At the M point, the two modes take the same value of the excitation energy 0.105 eV, while, at the X point, they take the energies nearly twice of that at the M point, which is in good accordance with the experiment. Notice that, within the analysis of the Heisenberg model on the basis of the localized picture, such result has been reproduced only when the second and third nearest-neighbor exchange terms were included in addition to the first nearest-neighbor exchange term.^{17,27} In the present treatment, however, since the hopping term between the nearest neighbor sites alone provides the desired results, the mechanism should be sought for different direction. It might be attributed to the mixing with high energy states. Examining the wavefunction at the X point, for example, we actually find that the hole sectors $|j_{\text{eff}} = \frac{3}{2}, +\frac{3}{2}\rangle$ and $|j_{\text{eff}} = \frac{3}{2}, -\frac{3}{2}\rangle$ with $\lambda = 1$ and 2 , respectively, have considerable amplitudes.

The dispersion curve agrees well with the recent RIXS experiment on the whole.¹⁷ It is remarkable that the RPA provides a good description of magnetic excitations without introducing ad hoc extended couplings in the Heisenberg model. Another remarkable point is the emergence of the gap mode. The present authors have recently analyzed the magnetic excitations within the strong coupling theory, and have predicted that the gap mode is brought about by the anisotropic exchange couplings.²⁷ Since the origin of the anisotropic exchange couplings is attributed to the interplay between Hund's coupling and the SOI, the gap modes in the itinerant electron description are considered to have the same origin. Although the existence of the gap mode has not been confirmed by experiments,^{17,28} the RIXS experiment seems promising with further improvement of energy resolution enough to detect the gap.²⁹

For ω around $\omega_B(\mathbf{q})$, $\hat{Y}(q)$ may be expressed as $\hat{Y}^T(q) = \hat{C}(\mathbf{q})/(\omega - \omega_B(\mathbf{q}) + i\delta)$. Then, the spectral function is given by

$$-2\text{Im} \sum_{\xi\xi'} [\hat{Y}^T(q)]_{\xi\xi',\xi\xi'} = 2\pi \sum_{\xi\xi'} [\hat{C}(\mathbf{q})]_{\xi\xi',\xi\xi'} \delta(\omega - \omega_B(\mathbf{q})). \quad (14)$$

We evaluate numerically the weight of the pole in Eq. (14), and obtain the integrated intensity I_B as $I_B = 2\pi \times 1.20$ at the X point, and $2\pi \times 0.96$ at the M point with summing up the intensities of two modes. Next, the spectral distribution of electron-hole pair creation is proportional to $-2\text{Im} \sum_{\xi\xi'} [\hat{Y}^T(q)]_{\xi\xi',\xi\xi'}$. In evaluating

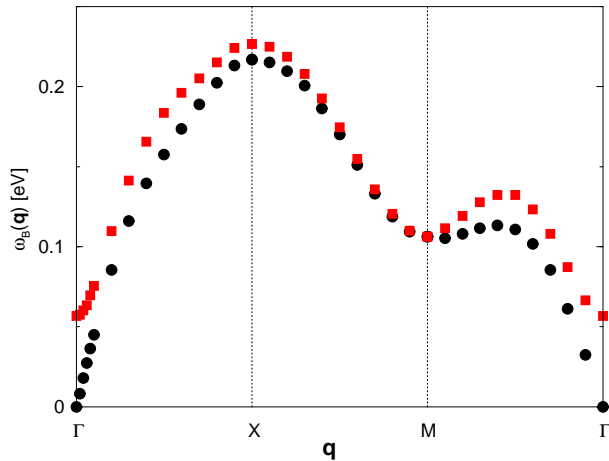


Figure 2: (Color online). Magnetic excitation energy for \mathbf{q} along the symmetry lines. $J/U = 0.15$.

this quantity, each $E_j(\mathbf{k} + \mathbf{q}) - E_\ell(\mathbf{k})$ inside the energy continuum in Eq. (13) is sorted into segments with the width of 0.005 eV for 300×300 \mathbf{k} -points, resulting in the histogram representation. Setting q_0 at the center of each segment, we evaluate Eq. (13) and thereby Eq. (12).

Figures 3(a) and (b) show the spectral functions evaluated at the Γ and X points, respectively, with and without Hund's coupling. When the multiple scattering is neglected, $\hat{Y}^T(q)$ is reduced to $\hat{F}(q)$. Then, the spectral function is given by $-2\text{Im} \sum_{\xi\xi'} [\hat{F}(q)]_{\xi\xi';\xi\xi'}$, which is shown by the thin lines (red). Its total intensity may be expressed as

$$I_{e-h} = -2\text{Im} \int_0^\infty \sum_{\xi\xi'} [\hat{F}(\mathbf{q}, \omega)]_{\xi\xi';\xi\xi'} d\omega. \quad (15)$$

Since ten states are occupied and two states are unoccupied per unit cell, we have $I_{e-h} = 2\pi \times 20$ with no \mathbf{q} -dependence.

When the multiple scattering is taken into account, the spectral weight is transferred to the lower energy region, leading to the decrease of intensity around $q_0 \sim 1$ eV as well as the split-off of intensity to the bound states. In addition, a new peak, which might be called as an exciton peak, surprisingly emerges as a resonant mode in the low energy region when Hund's coupling works. The integrated intensities around the peaks are estimated as $I_{\text{ex}} \sim 2\pi \times 1.25$ at the Γ point, $2\pi \times 2.12$ at the X point, and $2\pi \times 0.6$ and $2\pi \times 1.0$ for the two peaks at the M point.³⁰ Therefore the intensities of exciton peaks are the same order of magnitude as those of magnon peaks.

To search for the origin of the resonant mode, we examine the eigenvalues of $\hat{F}_1(q)^{-1} + \hat{\Gamma}$ at the peak energy with neglecting the small imaginary part $\hat{F}_2(q)$. We find that a couple of eigenvalues are quite close to zero, which we assign approximately as resonant modes. Two modes are obtained as resonant modes with a nearly degenerate energy at the X point, while the two modes are well separate with forming two peaks at the M point. At the first

sight, the amplitudes of the corresponding eigenstate are distributed on many base states, but by rewriting the base states in terms of eigenstates with $j_{\text{eff}} = \frac{1}{2}$ and $\frac{3}{2}$, we find at both points that the amplitudes are relatively large on the base states $|\frac{1}{2}, \frac{1}{2}\rangle|\frac{3}{2}, -\frac{3}{2}\rangle$ and $|\frac{1}{2}, \frac{1}{2}\rangle|\frac{3}{2}, +\frac{1}{2}\rangle$ with $\lambda = 1$, and $|\frac{1}{2}, -\frac{1}{2}\rangle|\frac{3}{2}, +\frac{3}{2}\rangle$ and $|\frac{1}{2}, -\frac{1}{2}\rangle|\frac{3}{2}, -\frac{1}{2}\rangle$ with $\lambda = 2$, where the front ket represents the excited-electron state and the rear ket does the hole state. The signs of the amplitudes for $\lambda = 1$ relative to those for $\lambda = 2$ are opposite between the two modes. Such exciton eigenstates contrast with the wavefunction of magnons, in which the hole sectors involve $|\frac{3}{2}, +\frac{3}{2}\rangle$ and $|\frac{3}{2}, -\frac{3}{2}\rangle$ with $\lambda = 1$ and 2, respectively. Unfortunately, the role of Hund's coupling on leading to such eigenstates is not clear.

Figure 3 (c) shows the spectral function as a function of q_0 along high symmetry directions with $J/U = 0.15$, which is convoluted with the Lorentzian function with the FWHM 0.04 eV. The exciton peak moves to lower energy region with changing \mathbf{q} from Γ to X as well as from Γ to M . This behavior is consistent with the observation in the RIXS experiment,¹⁷ although the spectra below $q_0 < 0.4$ eV around the M point have not been detected. It should be noted that the correlation function in the present definition may contain spectral intensities irrelevant to the RIXS spectra, since it has rather large integral intensity according to the sum-rule. For this reason, more quantitative analysis may be necessary, which is beyond the scope of the present study, since the RIXS spectra are not simply proportional to $-\text{Im} \sum_{\xi\xi'} [Y^T(q)]_{\xi\xi';\xi\xi'}$.²⁵ In the localized electron picture, the exciton peak is interpreted as the excitation from the $j_{\text{eff}} = \frac{3}{2}$ manifold to the $j_{\text{eff}} = \frac{1}{2}$ manifold, which requires the energy $\sim \frac{3}{2}\zeta_{\text{SO}}$ (~ 0.5 eV), and the dispersion as the hopping in the AFM isospin background.^{16,28} The $j_{\text{eff}} = \frac{3}{2}$ manifold in the present calculation forms broad bands with the width of ~ 1.5 eV, as shown in Fig. 1. The large amplitudes on the local excitation of $j_{\text{eff}} = \frac{3}{2} \rightarrow \frac{1}{2}$ found in the above analysis of eigenstates for excitons may partly correspond to the localized electron picture.

In summary, we have studied the elementary excitations in Sr_2IrO_4 on the viewpoint of itinerant electron picture. Introducing the multi-orbital Hubbard model, we have calculated the particle-hole Green's function within the HFA and RPA. We have obtained magnetic excitations as bound states with the dispersion relation in good accordance with the RIXS experiment. In addition, we have found that two new types of modes emerge due to the interplay between the SOI and Hund's coupling. One is the gap mode in the magnetic excitation, which is consistent with the prediction based on the localized electron picture.²⁷ Another is the exciton in the continuum of electron-hole pair excitation, which qualitatively captures a characteristic dependence on \mathbf{q} shown by the RIXS experiment. A next logical step will be to investigate the RIXS spectrum itself since it differs from the correlation function. Such a study has been carried out by the theory based on the localized spin picture, giving a qualitative agreement with the experiment.³¹ It

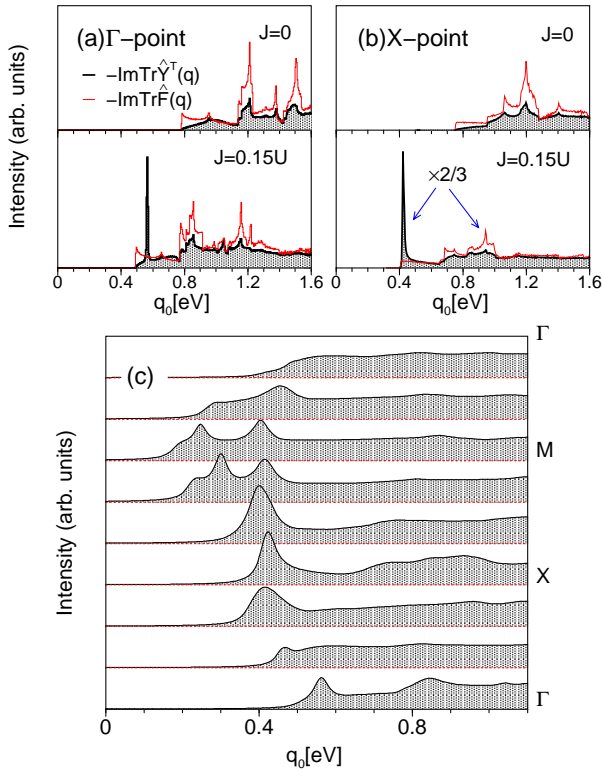


Figure 3: (Color online). The thick (black) line represents the spectral function $-\text{Im}\sum_{\xi\xi'}[\hat{Y}^T(q)]_{\xi\xi';\xi\xi'}$ of electron-hole pair creation in a fine scale. (a) At the Γ point and (b) X point. $J/U = 0$ (upper) and 0.15 (lower). The thin (red) line represents $-\text{Im}\sum_{\xi\xi'}[\hat{F}(q)]_{\xi\xi';\xi\xi'}$. (c) Spectral function as a function of q_0 with $J/U = 0.15$, which is convoluted with the Lorentzian function with the FWHM 0.04 eV.

is remarkable that a simple theory using the HFA and RPA provides a coherent description of elementary excitations comparable to experimental spectra. However, we need to refine the present model by including the crystal distortion for quantitative analysis. We hope our simple theoretical consideration would stimulate further research on Sr_2IrO_4 .

We are grateful to M. Yokoyama and T. Nomura for fruitful discussions. This work was partially supported by a Grant-in-Aid for Scientific Research from the Ministry of Education, Culture, Sports, Science and Technology of the Japanese Government.

- ¹ M. K. Crawford, M. A. Subramanian, R. L. Harlow, J. A. Fernandez-Baca, Z. R. Wang, and D. C. Johnston, Phys. Rev. B **49**, 9198 (1994).
- ² G. Cao, J. Bolivar, S. McCall, J. E. Crow, and R. P. Guertin, Phys. Rev. B **57**, R11039 (1998).
- ³ S. J. Moon, M. W. Kim, K. W. Kim, Y. S. Lee, J.-Y. Kim, J.-H. Park, B. J. Kim, S.-J. Oh, S. Nakatsuji, Y. Maeno, et al., Phys. Rev. B **74**, 113104 (2006).
- ⁴ J. P. Clancy, N. Chen, C. Y. Kim, W. F. Chen, K. W. Plumb, B. C. Jeon, T. W. Noh, and Y. -J. Kim, Phys. Rev. B **86**, 195131 (2012).
- ⁵ D. Haskel, G. Fabbris, M. Zhernenkov, P. P. Kong, C. Q. Jin, G. Cao, and M. van Veenendaal, Phys. Rev. Lett. **109**, 027204 (2012).
- ⁶ F. Ye, S. Chi, B. C. Chakoumakos, J. A. Fernandez-Baca, T. Qi, and G. Cao, Phys. Rev. B **87**, 140406(R) (2013).
- ⁷ H. Watanabe, T. Shirakawa, and S. Yunoki, Phys. Rev. Lett. **110**, 027002 (2013).
- ⁸ J.-M. Carter, V. V. Shankar, and H.-Y. Kee, Phys. Rev. B **88**, 035111 (2013).
- ⁹ Y. Singh and P. Gegenwart, Phys. Rev. B **82**, 064412 (2010).
- ¹⁰ Y. Singh, S. Manni, J. Reuther, T. Berlijn, R. Thomale, W. Ku, S. Trebst, and P. Gegenwart, Phys. Rev. Lett. **108**, 127203 (2012).
- ¹¹ J. Chaloupka, G. Jackeli, and G. Khaliullin, Phys. Rev. Lett. **110**, 097204 (2013).
- ¹² F. Trouselet, M. Berciu, A. M. Oleś, and P. Horsch, Phys. Rev. Lett. **111**, 037205 (2013).
- ¹³ B. J. Kim, H. Jin, S. J. Moon, J.-Y. Kim, B.-G. Park, C. S. Leem, J. Yu, T. W. Noh, C. Kim, S.-J. Oh, et al., Phys. Rev. Lett. **101**, 076402 (2008).
- ¹⁴ B. J. Kim, H. Ohsumi, T. Komesu, S. Sakai, T. Morita, H. Takagi, and T. Arima, Science **323**, 1329 (2009).
- ¹⁵ G. Jackeli and G. Khaliullin, Phys. Rev. Lett. **102**, 017205 (2009).
- ¹⁶ B. H. Kim, G. Khaliullin, and B. I. Min, Phys. Rev. Lett. **109**, 167205 (2012).
- ¹⁷ J. Kim, D. Casa, M. H. Upton, T. Gog, Y.-J. Kim, J. F. Mitchell, M. van Veenendaal, M. Daghofer, J. van den Brink, G. Khaliullin, et al., Phys. Rev. Lett. **108**, 177003 (2012).
- ¹⁸ L. Braicovich, L. J. P. Ament, V. Bisogni, F. Forte, C. Aruta, G. Balestrino, N. B. Brookes, G. M. D. Luca, P. G. Medaglia, F. M. Granozio, et al., Phys. Rev. Lett. **102**, 167401 (2009).

- ¹⁹ M. Guarise, B. D. Piazza, M. M. Sala, G. Ghiringhelli, L. Braicovich, H. Berger, J. N. Hancock, D. van der Marel, T. Schmitt, V. N. Strocov, et al., *Phys. Rev. Lett.* **105**, 157006 (2010).
- ²⁰ R. Arita, J. Kuneš, A. V. Kozhevnikov, A. G. Eguiluz, and M. Imada, *Phys. Rev. Lett.* **108**, 086403 (2012).
- ²¹ S. Moser, L. Moreschini, A. Ebrahimi, B. D. Piazza, M. Isobe, H. Okabe, J. Akimitsu, V. V. Mazurenko, K. S. Kim, A. Bostwick, et al., *New J. Phys.* **16**, 013008 (2014).
- ²² H. Watanabe, T. Shirakawa, and S. Yunoki, *Phys. Rev. Lett.* **105**, 216410 (2010).
- ²³ F. Wang and T. Senthil, *Phys. Rev. Lett.* **106**, 136402 (2011).
- ²⁴ J. Kanamori, *Prog. Theor. Phys.* **30**, 275 (1963).
- ²⁵ J. I. Igarashi and T. Nagao, *Phys. Rev. B* **88**, 014407 (2013).
- ²⁶ For $H_I = \frac{1}{2} \sum_{\nu_1 \nu_2 \nu_3 \nu_4} g(\nu_1 \nu_2; \nu_3 \nu_4) d_{\nu_1}^\dagger d_{\nu_2}^\dagger d_{\nu_4} d_{\nu_3}$ with $\nu = (n\sigma)$, the antisymmetric vertex function $\Gamma^{(0)}$ is defined as $\Gamma^{(0)}(\xi_1 \xi_2; \xi_3 \xi_4) = g(\xi_1 \xi_2; \xi_3 \xi_4) - g(\xi_1 \xi_2; \xi_4 \xi_3)$, with $\xi_n = (\lambda_n, \nu_n)$. It gives non-zero value only when $\lambda_1 = \lambda_2 = \lambda_3 = \lambda_4$.
- ²⁷ J. I. Igarashi and T. Nagao, *Phys. Rev. B* **88**, 104406 (2013).
- ²⁸ L. J. P. Ament, G. Khaliullin, and J. van den Brink, *Phys. Rev. B* **84**, 020403 (2011).
- ²⁹ M. M. Sala, C. Henriquet, L. Simonelli, R. Verbeni, and G. Monaco, *J. Electron Spectrosc. Relat. Phenom.* **188**, 150 (2013).
- ³⁰ The definition of the integrated intensity of exciton peaks is ambiguous. We sum up intensities in the region $(\omega_0 - 0.2, \omega_0 + 0.2)$ (eV) with ω_0 being the peak position.
- ³¹ J. I. Igarashi and T. Nagao, *Phys. Rev. B* **89**, 064410 (2014).